Mathematics

https://www.aimspress.com/journal/Math

AIMS Mathematics, 11(7): 22004–22033.
DOI: 10.3934/math.2026890
Received: 10 February 2026
Revised: 05 July 2026
Accepted: 14 July 2026
Published: 23 July 2026

Research article

Optimal reconstruction of spatial sources for a dynamical problem characterized by a space–time fractional diffusion–wave model

Maawiya Ould Sidi[1,*], Mofareh Alhazmi[1], Mustapha Benoudi[2], Kareem Alanazi[1], Abdeldjalil Chattouh[3] and Hamed Ould Sidi[4]

[1] Department of Mathematics, College of Science, Jouf University, Sakaka, Aljouf 72341, Saudi Arabia

[2] Laboratory of Research in Engineering Sciences and Innovation, National School of Applied Sciences of Beni-Mellal, Sultan Moulay Slimane University, Beni-Mellal, 23000, Morocco

[3] Department of Mathematics, Abbes Laghrour University of Khenchela, Khencheka, Algeria

[4] Institut Supérieur de Comptabilité et d'Administration des Entreprises- ISCAE Nouakchott, Mauritania

* **Correspondence:** Email: msidi@ju.edu.sa.

Abstract: This paper addresses the optimal recovery of spatial sources in a dynamical problem governed by a space-time fractional diffusion-wave model. Specifically, we estimate the spatial component of the source term from final-time observations in a bounded domain. Such inverse source problems are inherently ill-posed and require additional information here provided by the final-time measurements to guarantee uniqueness. To this end, we propose a nonlinear optimization formulation that provides a stable and effective framework for source identification. Given the sensitivity of the problem to data perturbations, we employ Tikhonov regularization to stabilize the reconstruction. The proposed methodology minimizes a least-squares cost functional that quantifies the mismatch between the model output and the measured final-time data, augmented with a regularization term to control instability and ensure well-posedness. We prove the Fréchet differentiability of the resulting functional and derive an adjoint-based gradient expression, enabling efficient implementation. The numerical solution is obtained using a conjugate gradient algorithm, with the Morozov discrepancy principle used to guide the stopping criterion. A series of one-dimensional numerical experiments is performed to demonstrate the effectiveness of the proposed method. The results confirm the robustness, accuracy, and computational efficiency of the proposed strategy for source reconstruction in fractional-order dynamical systems.

Keywords: fractional Laplacian operator; fractional calculus; inverse problem
Mathematics Subject Classification: 35R11, 35L05, 35R30, 47A52

1. Introduction

The landscape of scientific and engineering modeling has been transformed by the advent of fractional-order operators, which have proven invaluable for capturing phenomena that lie beyond the reach of traditional operators. The fractional Laplacian, in particular, has revolutionized the modeling of diffusion processes. The theoretical foundation of this operator is rooted in probability theory and emerges naturally as the limiting case of extended-range random walks [1].

The versatility of fractional models has led to their widespread adoption in various scientific domains. Their applications span multiple disciplines, including the analysis of anomalous diffusion patterns [2] and the study of geophysical phenomena [3]. In the realm of image processing and materials science, these models have proven instrumental for denoising applications and phase-field modeling [4]. Their utility extends further to the analysis of fluid dynamics in porous media [5], the processing of complex datasets [6], the study of elastic properties in materials [7], and the modeling of population dynamics in biological systems [8].

This remarkable breadth of applications underscores how fractional operators have evolved from mathematical curiosities into essential tools for understanding complex natural phenomena that defy conventional analytical approaches.

In recent years, inverse source problems (ISPs) associated with both integer-order and fractional partial differential equations have attracted increasing attention due to their wide range of applications in science and engineering. Several approaches have been proposed to address these problems under different modeling assumptions. Murio et al. [9] proposed a regularization-based strategy for estimating unknown source terms from discrete measurement data. The issue of uniqueness was investigated by Nakagawa et al. [10], who showed that an ISP can be uniquely solved using observations collected over a restricted space–time domain. Applications to environmental modeling were considered by Anderle et al. [11], where pollution source identification was studied within the framework of the heat equation. In a biomedical context, El Badia et al. [12] developed a method for locating electrostatic dipoles in the human brain. More recently, Bensalah et al. [13] examined an ISP governed by a space–time fractional diffusion equation, with particular emphasis on identifying the spatial component of the source term from partial observations. Furthermore, Sidi et al. [14] investigated a time–space fractional diffusion ISP using final-time data and employed a combination of nonstationary iterative Tikhonov regularization and classical Tikhonov regularization to enhance solution stability.

Ali et al. [15] investigated two inverse source problems arising from a space–time fractional differential equation, each involving a different type of unknown source term. In the first setting, the authors considered the recovery of a spatially varying source, whereas the second problem concerned the identification of a temporally dependent source function. Their solution methodology relies on a biorthogonal family of functions constructed from Mittag–Leffler-type functions, derived via the spectral analysis of the fractional operator and its corresponding adjoint problem. For the inverse problem with a space-dependent source term, the authors established rigorous results on existence, uniqueness, and stability. In contrast, the time-dependent source problem was shown to admit a unique solution under appropriate assumptions. In addition, several illustrative examples were presented to demonstrate the applicability of the proposed approach.

In this work, we explore the inverse problem of reconstructing an unknown source in a space–

time fractional diffusion–wave equation. Reconstructing unknown sources is a fundamental challenge in applied sciences, aimed at extracting precise information about physical phenomena or objects from observational data and experimental measurements. This problem is of paramount importance in a wide range of practical applications, including engineering sciences, geophysical prospecting, electromagnetic theory, and pollutant detection. It also plays a vital role in the development of medical imaging techniques, the analysis of environmental systems, the monitoring of groundwater quality, and the evaluation of the dispersion of air and soil pollution. In addition, this inverse problem has significant implications for monitoring structural health, detecting material defects, and remote sensing. Understanding and solving such inverse problems contribute substantially to the development of effective solutions for practical challenges across various scientific and industrial domains.

The complexity of this reconstruction process lies in its ill-posed nature, which requires sophisticated mathematical techniques and computational methods to obtain stable and meaningful solutions. The space–time fractional approach provides a more comprehensive framework for modeling complex diffusion and wave phenomena, capturing memory effects and spatial heterogeneity that traditional integer-order models may overlook. This enhanced modeling capability is particularly valuable in applications where classical diffusion theories fail to adequately describe observed physical behavior.

The main contributions of this work can be summarized as follows:

Theoretical contributions:

1. We establish the existence, uniqueness, and stability of the solution to the inverse source problem for a space–time fractional diffusion–wave equation.
2. The ill-posed nature of the problem is rigorously addressed through a Tikhonov regularization framework, for which we prove well-posedness and stability with respect to noisy final-time measurements.
3. We establish the Fréchet differentiability of the associated cost functional and derive an explicit adjoint-based expression for its gradient, which allows efficient implementation within iterative optimization algorithms.
4. A convergence analysis is carried out for the finite element discretization, ensuring that the numerical approximation inherits the stability and accuracy guarantees of the continuous problem.

Numerical contributions:

1. We design an iterative recovery algorithm using the conjugate gradient method (CGM), coupled with the adjoint problem, to improve computational efficiency.
2. The method is implemented using a fully discrete scheme that combines finite difference time stepping with a finite element discretization of the fractional Laplacian.
3. Extensive numerical experiments, including smooth, nonsmooth, and piecewise-defined source terms, are performed under various noise levels. The results demonstrate robustness, accuracy, and stability, even for highly perturbed data, and confirm the practical applicability of the proposed approach.

These contributions extend and complement previous works such as [13–15], particularly by providing stronger stability guarantees and practical reconstruction strategies in noisy environments.

The rest of the article is organized as follows. Section 2 introduces the notation and presents the main preliminary results needed for the analysis. Section 3 is devoted to the uniqueness of the inverse problem and its reformulation as an optimization problem. Section 4 describes the conjugate gradient algorithm, developed from the corresponding adjoint problems. In Section 5, we apply the finite element method to approximate the variational problem and establish convergence of the proposed numerical scheme. Finally, Section 6 presents a series of numerical experiments illustrating the effectiveness and accuracy of the proposed approach.

2. Basic concepts

This section introduces the fundamental definitions required for the remainder of the paper.

Definition 2.1. [16, 17] Let $\nu > 0$. The Riemann–Liouville fractional integral of order ν of a function Ψ is defined as

$$\mathcal{I}_0^{\nu}\Psi(t) = \frac{1}{\Gamma(\nu)}\int_0^t (t-\zeta)^{\nu-1}\Psi(\zeta)\,d\zeta \tag{2.1}$$

Definition 2.2. [16, 17] Let $n-1 \le \nu < n$. The Caputo fractional derivative of order ν is given by

$$\mathcal{D}_t^{\nu}\Psi(t) = \mathcal{I}_0^{n-\nu}\Psi^{(n)}(t) = \frac{1}{\Gamma(n-\nu)}\int_0^t (t-\zeta)^{n-1-\nu}\Psi^{(n)}(\zeta)\,d\zeta. \tag{2.2}$$

Definition 2.3. [16, 17] For an order β, the Riemann-Liouville derivative is defined with $m-1 \le \beta < m$ as follows:

$$\mathcal{D}_t^{\beta}\Psi(t) = \frac{d^m}{dt^m}\mathcal{I}_0^{m-\beta}\Psi(t) = \frac{1}{\Gamma(m-\beta)}\frac{d^m}{dt^m}\int_0^t (t-q)^{m-1-\beta}\Psi(q)\,dq. \tag{2.3}$$

Given $T > 0$ and a bounded domain $\Omega \subset \mathbb{R}^m$, we consider the following system governed by a Caputo fractional derivative of order $\nu \in (1,2)$:

$$\begin{cases} {}^{C}D_t^{\nu}\varrho(x,t) = (-\Delta)^s\varrho(x,t) + g(x)h(t) & (x,t) \in \Omega\times(0,T), \\ \varrho(\xi,t) = 0 & \partial\Omega\times(0,T), \\ \varrho(x,0) = \varrho_0(x), \quad \dfrac{\partial\varrho}{\partial t}(x,0) = \varrho_1(x), & x \in \Omega. \end{cases} \tag{2.4}$$

For ($s \in (0,1)$), we define the fractional Laplacian operator by

$$(-\Delta)^s\varrho(x,t) = C_{m,s}\,\mathrm{P.V.}\int_{\mathbb{R}^m}\frac{\varrho(x,t)-\varrho(y,t)}{|x-y|^{m+2s}}\,dy, \tag{2.5}$$

where $g \in L^2(\Omega)$, $h \in L^2(0,T)$, and $C_{m,s}$ is a normalization constant given by

$$C_{m,s} = \frac{4^s s\,\Gamma\!\left(s+\frac{m}{2}\right)}{\pi^{\frac{m}{2}}\Gamma(1-s)}.$$

The Cauchy principal value (P.V.) is

$$\mathrm{P.V.}\int_{\mathbb{R}^m}\frac{\varrho(x,t)-\varrho(y,t)}{|x-y|^{m+2s}}\,dy = \lim_{\delta\to 0}\int_{\{y\in\mathbb{R}^m:\,|y-x|>\delta\}}\frac{\varrho(x,t)-\varrho(y,t)}{|x-y|^{m+2s}}\,dy.$$

Next, we introduce some notations and recall the standard functional spaces used throughout the paper. The space $L^2(\Omega)$ is equipped with the usual inner product $(\cdot,\cdot)$, while $H^1(\Omega)$, $H_0^1(\Omega)$, $H^s(0,T)$, and related spaces denote Sobolev spaces (see Adams [18]).

The fractional Sobolev space is given by

$$H_0^s(\Omega) := \left\{\varrho \in W^{s,2}(\mathbb{R}^m) : \varrho = 0 \text{ a.e. in } \mathbb{R}^m \setminus \Omega\right\}, \quad s \in (0,1).$$

and the associated norm is

$$\|\varrho\|_{H_0^s(\Omega)} := \left(\int_{\mathbb{R}^m}\int_{\mathbb{R}^m} \frac{|\varrho(x)-\varrho(y)|^2}{|x-y|^{m+2s}}\,dx\,dy\right)^{1/2}.$$

Using the Fourier transform $\mathcal{F}$, the Sobolev space $W^{s,2}(\mathbb{R}^m)$ is defined by

$$W^{s,2}(\mathbb{R}^m) := \left\{\varrho \in L^2(\mathbb{R}^m) : (1+|\xi|^2)^{s/2}\mathcal{F}\varrho \in L^2(\mathbb{R}^m)\right\}.$$

We define the space $H^s(\Omega)$ by

$$H^s(\Omega) := \left\{\varrho \in L^2(\Omega) : |\varrho|_{H^s(\Omega)} < \infty\right\},$$

where the Gagliardo seminorm is given by

$$|\varrho|_{H^s(\Omega)} := \left(\int_{\Omega}\int_{\Omega} \frac{|\varrho(x)-\varrho(y)|^2}{|x-y|^{m+2s}}\,dx\,dy\right)^{1/2}.$$

The corresponding norm in $H^s(\Omega)$ is

$$\|\varrho\|_{H^s(\Omega)} := \left(\|\varrho\|^2_{L^2(\Omega)} + |\varrho|^2_{H^s(\Omega)}\right)^{1/2}.$$

Furthermore, for $s \in (0,1)$, we introduce the fractional space

$$\widetilde{H}^s(\Omega) := \left\{\varrho \in H^s(\mathbb{R}^m) : \operatorname{supp}(\varrho) \subset \overline{\Omega}\right\}.$$

The bilinear form related to the space $H^s(\Omega)$ is given by

$$B_s(\varrho,\Phi) := C_{m,s}\iint_{(\mathbb{R}^m\times\mathbb{R}^m)\setminus(\Omega^c\times\Omega^c)} \frac{(\varrho(x)-\varrho(y))(\Phi(x)-\Phi(y))}{|x-y|^{m+2s}}\,dx\,dy.$$

Proposition 2.1. *(see [19]). Let $\varrho,\ \Phi : \mathbb{R}^m \to \mathbb{R}$ be infinitely differentiable functions. Then,*

$$\int_{\Omega} \Phi(x)(-\Delta)^s\varrho(x)dx = \frac{B_s(\varrho,\ \Phi)}{2} - \int_{\Omega^c} \Phi(x)\mathcal{N}_s\varrho(x)dx.$$

Here, the nonlocal Neumann operator $\mathcal{N}_s$ related to the fractional Laplacian $(-\Delta)^s$ is

$$\mathcal{N}_s\varrho(x) = C_{m,s}\int_{\Omega} \frac{\varrho(x)-\varrho(y)}{|x-y|^{m+2s}}\,dy.$$

The link between the fractional Riemann–Liouville derivative and the fractional Caputo derivative is established using a fractional integration-by-parts formula. This fundamental result provides a direct connection between these two notions and plays a central role in the analysis of fractional differential equations.

Proposition 2.2. *Let $\nu \in (1,2)$ and let ϱ_1 and ϱ_2 be absolutely integrable functions. Then, we have*

$$\int_0^T \varrho_2(t)\, {}^{C}\mathrm{D}_t^{\nu}\varrho_1(t)\,dt = \int_0^T \varrho_1(t)\, {}^{RL}\mathrm{D}_t^{\nu}\varrho_2(t)\,dt + \left[\varrho_1(t)\frac{\partial}{\partial t}\mathrm{I}_t^{2-\nu}\varrho_2(t)\right]_{t=0}^{t=T} - \left[\mathrm{I}_t^{2-\nu}\varrho_2(t)\frac{\partial \varrho_1}{\partial t}(t)\right]_{t=0}^{t=T}.$$

Definition 2.4. [20] A collection of bounded linear operators $\{C(t)\}_{t\in\mathbb{R}}$ acting on $H^s(\Omega)$ is called a strongly continuous cosine operator family if it satisfies the following conditions: $C(0)$ coincides with the identity operator on $H^s(\Omega)$; the functional relation

$$C(t+s) + C(t-s) = 2\,C(t)C(s) \quad \text{for all } t, s \in \mathbb{R}$$

holds; and for every $\varrho \in H^s(\Omega)$, the mapping $t \mapsto C(t)\varrho$ is continuous with respect to the norm of $H^s(\Omega)$.

Associated with the cosine operator family $\{C(t)\}_{t\in\mathbb{R}}$, we define the strongly continuous sine family $\{S(t)\}_{t\in\mathbb{R}}$ by

$$S(t)\varrho := \int_0^t C(\zeta)\varrho\, d\zeta, \qquad \varrho \in H^s(\Omega),\ t \in \mathbb{R}.$$

Moreover, the operator $A = (-\Delta)^s$ is referred to as the infinitesimal generator of the cosine operator family $\{C(t)\}_{t\in\mathbb{R}}$ if the second derivative of $C(t)\varrho$ at $t = 0$ exists for all $\varrho \in \mathcal{D}(A)$ and satisfies

$$A\varrho = \frac{d^2}{dt^2}\, C(t)\varrho\Big|_{t=0}.$$

The domain $\mathcal{D}(A) \subset H^s(\Omega)$ consists of all elements ϱ for which the above limit is well defined in $H^s(\Omega)$.

$$\mathcal{D}(A) = \{\varrho \in H^s(\Omega) : C(t)\varrho \in C^2(\mathbb{R},\ H^s(\Omega))\}.$$

Definition 2.5. We say that $\varrho \in C((0,T); H_0^s(\Omega)) \cap C^1([0,T]; L^2(\Omega))$ provides a *mild solution* to problem (2.4) if the initial conditions

$$\varrho(0) = \varrho_0, \qquad \frac{\partial \varrho}{\partial t}(0) = \varrho_1,$$

are satisfied and the following integral representation holds:

$$\varrho(x,t) = S_\nu(t)\varrho_0(x) + P_\nu(t)\varrho_1(x) + g(x)\int_0^t (t-r)^{\nu-1} K_\nu(t-r)\, h(r)\, dr, \tag{2.6}$$

where

$$S_{\nu}(t) = \int_0^{\infty} M_{\nu}(\theta)C(t^{\nu}\theta)\,d\theta, \quad P_{\nu}(t) = \int_0^{t} S_{\nu}(r)\,dr, \quad \text{and} \quad K_{\nu}(t) = \int_0^{\infty} \nu\theta M_{\nu}(\theta)S(t^{\nu}\theta)\,d\theta.$$

The $M_{\nu}(\theta)$ function is given by

$$M_{\nu}(\theta) = \frac{1}{\nu}\theta^{-\nu-1}\Psi_{\nu}\left(\theta^{-\frac{1}{\nu}}\right), \quad \Psi_{\nu}(\theta) = \frac{1}{\pi}\sum_{n=1}^{\infty}(-1)^{n-1}\theta^{-n\nu-1}\frac{\Gamma(n\nu+1)}{n!}\sin(n\pi\nu).$$

The parameter θ takes values in $(0,\infty)$, and $M_{\nu}(\cdot)$ denotes the Mainardi Wright-type function. This function is nonnegative on $(0,\infty)$ and normalized in the sense that

$$\int_0^{\infty} M_{\nu}(\theta)\,d\theta = 1.$$

Remark 2.1. The operator $(-\Delta)^s$ admits a complete orthonormal basis of eigenfunctions (ϑ_n) associated with a sequence of eigenvalues (Υ_n). Consequently, the mild solution to problem (2.4) can be represented as follows:

$$\varrho(x,t) = \sum_{n=0}^{+\infty}\left[E_{\nu,1}(-\Upsilon_n t^{\nu})\langle\varrho_0,\ \vartheta_n\rangle + tE_{\nu,2}\left(-\Upsilon_n t^{\nu}\right)\langle\varrho_1,\ \vartheta_n\rangle\right]\vartheta_n \tag{2.7}$$

$$+\sum_{n=0}^{+\infty}\int_0^{t}\left[(t-r)^{\nu-1}h(r)E_{\nu,\nu}(-\Upsilon_n(t-r)^{\nu})\langle g,\ \vartheta_n\rangle\right]\vartheta_n\,dr, \tag{2.8}$$

where $E_{\nu,\beta}(z) = \sum_{n=0}^{+\infty}\frac{z^n}{\Gamma(\beta+n\nu)}$ is the Mittag Leffler function.

The solution of the direct problem (2.4) can be represented using the properties of this family of functions.

Lemma 2.1. *[14] Consider $\nu > 0$ and $\Upsilon > 0$. Then, we deduce*

$${}^{C}\mathrm{D}_t^{\nu}E_{\nu,1}(-\Upsilon t^{\nu}) = -\Upsilon E_{\nu,1}(-\Upsilon t^{\nu}), \quad t > 0. \tag{2.9}$$

In addition, the following identity is satisfied in the case of integer-order differentiation:

$$\frac{d}{dt}E_{\nu,1}(-\Upsilon t^{\nu}) = -\Upsilon t^{\nu-1}E_{\nu,\nu}(-\Upsilon t^{\nu}), \quad t > 0. \tag{2.10}$$

Lemma 2.2. *Let $1 < \nu < 2$. Then, there exists a constant $C_0 = C_0(\nu) > 0$ such that*

$$|E_{\nu,1}(z)| \leq \frac{C_0}{1+|z|}, \quad |\arg(z)| \leq \pi, \tag{2.11}$$

and

$$|E_{\nu,2}(z)| \leq \frac{C_0}{1+|z|^2}, \quad |z| \to +\infty. \tag{2.12}$$

3. Formulation and analysis of an inverse source problem

This section presents a mathematical analysis of the ISP associated with the fractional hyperbolic space–time equation (2.4). We derive theoretical results ensuring the existence and uniqueness of the solution.

An initial approximation $g \in L^2(\Omega)$ of the unknown source g^* is considered, and $\varrho[g]$ denotes the solution of the corresponding fractional parabolic problem.

$$\begin{cases} {}^C D_t^\gamma \varrho[g](x,t) = (-\Delta)^s \varrho[g](x,t) + g(x)h(t), & (x,t) \in \Omega \times (0,T), \\ \varrho[g](\xi,t) = 0, & \partial\Omega \times (0,T), \\ \varrho[g](x,0) = 0, \quad \dfrac{\partial \varrho[g]}{\partial t}(x,0) = 0, & x \in \Omega. \end{cases} \tag{3.1}$$

The final observation $V(x) = \varrho(x,T)$ is assumed to be known, where ϱ denotes the potential associated with the true spatial source g^* and satisfies system (2.4). The inverse problem is to identify $g \in L^2(\Omega)$ such that the associated potential $\varrho[g](x,T)$ approximates the experimental data V in Ω. To this end, a bounded linear operator Π is introduced such that

$$\begin{array}{rccc} \Pi \ : & L^2(\Omega) & \to & L^2(\Omega) \\ & g(x) & \mapsto & \varrho[g](x,T). \end{array} \tag{3.2}$$

Using the final-time data V, one may estimate the true space-dependent component g^*. In practical applications, however, the measured data V are generally not exact, as noise is inherently associated with any measurement process. Therefore, we introduce V^δ, the final-time observation data satisfying

$$\|V(x) - V^\delta(x)\|_{L^2(\Omega)} \leq \delta, \tag{3.3}$$

where $\delta > 0$ denotes the noise level.

In general, this problem is ill-posed in the sense of Hadamard. Reconstruction stability is particularly problematic when noise is present. In this work, we address the numerical instability of the inverse problem by adopting a least-squares framework combined with Tikhonov regularization. Specifically, the approach consists in minimizing the following functional:

$$(IP) \begin{cases} \text{Find } g^* \in L^2(\Omega) \text{ where} \\ Q(g^*) = \min\limits_{g \in L^2(\Omega)} \dfrac{1}{2} \left\{ \|\Pi g(x) - V^\delta(x)\|^2_{L^2(\Omega))} + \eta \|g(x)\|^2_{L^2(\Omega)} \right\}. \end{cases} \tag{3.4}$$

The parameter η is the Tikhonov regularization parameter. The existence and stability results for the minimizer of (3.4) can be established by arguments analogous to those used in ([21], Theorems 4.3 and 4.4).

Theorem 3.1. *For every regularization parameter $\eta > 0$, the optimization problem* (3.4) *admits a unique minimizer. In particular, the regularized formulation yields a unique solution associated with* (3.4).

Theorem 3.2. *Let $\{V_n\} \subset L^2(\Omega)$ be a sequence of observation data converging to V^δ in $L^2(\Omega)$ as $n \to \infty$. For each n, let g_n denote the minimizer of the functional $\mathcal{Q}(g)$ associated with problem* (3.4)*, where V^δ is replaced by V_n. Then the sequence $\{g_n\}$ converges to the regularized solution corresponding to the data V^δ. This implies continuous dependence of the regularized solution on the data, ensuring stability under perturbations of V^δ.*

This paragraph is devoted to the analysis of the uniqueness of the inverse problem. In particular, we show that the space-dependent source g^* is uniquely determined from the final-time observation $\varrho(\cdot, T)$.

Theorem 3.3. *Let $h \in C([0, T])$ be a non zero non negative function. Let ϱ_ℓ with $\ell = 1, 2$ be the solutions of the problems*

$$\begin{cases} {}^C\mathrm{D}_t^\nu \varrho_\ell + (-\Delta)^s \varrho_\ell = g_\ell^* h & in \ \ \Omega \times (0, T], \\ \varrho_\ell = 0 & in \ \ \partial\Omega \times (0, T], \\ \varrho_\ell(x, 0) = 0, \quad \dfrac{\partial \varrho_\ell}{\partial t}(x, 0) = 0, & x \in \Omega, \end{cases} \tag{3.5}$$

with $g_\ell^* \in L^2(\Omega)$ and the condition

$$\varrho_1(\cdot, T) = \varrho_2(\cdot, T) \ in \ \ \Omega. \tag{3.6}$$

Then, we have

$$g_1^* = g_2^* \ in \ \ L^2(\Omega). \tag{3.7}$$

Proof. We consider two functions $\varrho_1(x, t)$ and $\varrho_2(x, t)$. Then, we have

$$\varrho_1(x, T) = \sum_{n=0}^{+\infty} \int_0^T \left[(T - r)^{\nu - 1} h(r) E_{\nu,\nu}(-\Upsilon_n (T - r)^\nu) \langle g_1^*, \ \vartheta_n \rangle \right] \vartheta_n \, dr,$$

and

$$\varrho_2(x, T) = \sum_{n=0}^{+\infty} \int_0^T \left[(T - r)^{\nu - 1} h(r) E_{\nu,\nu}(-\Upsilon_n (T - r)^\nu) \langle g_2^*, \ \vartheta_n \rangle \right] \vartheta_n \, dr.$$

Since the final measurements satisfy $\varrho_1(x, T) = \varrho_2(x, T)$, it follows that

$$\begin{aligned} &\sum_{n=0}^{+\infty} \int_0^T \left[(T - r)^{\nu - 1} h(r) E_{\nu,\nu}(-\Upsilon_n (T - r)^\nu) \langle g_1^*, \ \vartheta_n \rangle \right] \vartheta_n \, dr \\ &= \sum_{n=0}^{+\infty} \int_0^T \left[(T - r)^{\nu - 1} h(r) E_{\nu,\nu}(-\Upsilon_n (T - r)^\nu) \langle g_2^*, \ \vartheta_n \rangle \right] \vartheta_n \, dr. \end{aligned}$$

By the orthonormality of the basis $\{\vartheta_n\}$, we can equate the coefficients corresponding to each ϑ_n. For each n, this gives

$$\sum_{n=0}^{+\infty} \int_0^T \left[(T - r)^{\nu - 1} h(r) E_{\nu,\nu}(-\Upsilon_n (T - r)^\nu) \langle g_1^*, \vartheta_n \rangle \right] dr$$

$$= \sum_{n=0}^{+\infty} \int_0^T \left[(T-r)^{\nu-1} h(r) E_{\nu,\nu}(-\Upsilon_n (T-r)^{\nu}) \langle g_2^*,\ \vartheta_n \rangle \right] dr.$$

By identifying the Fourier coefficients, and since $h(r)$, $(T-r)^{\nu-1}$, and $E_{\nu,\nu}(-\Upsilon_n(T-r)^{\nu})$ are independent of g_1^* and g_2^*, we can write

$$\langle g_1^*,\ \vartheta_n \rangle = \langle g_2^*,\ \vartheta_n \rangle, \quad \forall n \geq 0.$$

It follows that:

$$g_1^*(x) = g_2^*(x).$$

□

This subsection also discusses stability. We study the behavior of the problem under small deviations in the observed measurements. To this end, let $\{V_k^{\delta}\}_{k\geq 1}$ satisfy

$$V_k^{\delta} \longrightarrow V^{\delta} \quad \text{in } L^2(\Omega) \text{ as } k \to \infty, \tag{3.8}$$

and consider a corresponding family $\{g^k\}$ associated with these perturbed problems.

$$\min_{g \in L^2(\Omega)} Q_k(g), \quad Q_k(g) := \|\varrho(g) - V_k^{\delta}\|^2_{L^2(\Omega)} + \eta \|g\|^2_{L^2(\Omega)}, \quad k = 1, 2. \tag{3.9}$$

The following minimization problem has a unique solution for each $k \geq 1$, which is g^k.

$$(IP)^k \qquad \inf_{g \in L^2(D)} Q_k(g).$$

Theorem 3.4. *The sequence of minimizers $\{g^k\}_{k\geq 1}$ is strongly convergent in $L^2(\Omega)$. More precisely, there exists a function $g^* \in L^2(\Omega)$ such that*

$$\|g^k - g^*\|_{L^2(\Omega)} \longrightarrow 0 \quad \text{as } k \to \infty. \tag{3.10}$$

In conclusion, the limit g^* is the unique solution to (IP). This result shows that the inverse problem is resilient to inaccuracies in the observed data.

Proof. According to Lemma 3.1 in [13], there exists a sequence of functions $\{g^k\}_{k\geq 1}$ such that, for every $k \geq 1$, the following property holds:

$$Q_k(g^k) \leq Q_k(g), \quad \forall g \in L^2(\Omega).$$

Thus, $\{g^k\}_{k\geq 1}$ is uniformly bounded. Consequently, there exist $g^{\#}$ and a subsequence of $\{g^k\}_{k\geq 1}$, still denoted by $\{g^k\}$, using Proposition 3.2 (see [13]), such that

$$g^k \to g^{\#} \quad \text{in } L^2(\Omega) \quad \text{as } k \to \infty.$$

The following can be obtained by applying the same method as in the proof of Theorem 3.5 (see [13]):

$$\varrho(g^k) \to \varrho(g^{\#}) \quad \text{in } X^{\nu,s}(0,T;\ L^2(\Omega)) \quad \text{as } k \to \infty,$$

where $X^{\nu,s}(0,T;\ L^2(\Omega)) = L^2(0,T;\ \widetilde{H}^s(\Omega) \cap H^{s+\gamma}(\Omega)) \cap {}_0H^\nu(0,T;\ L^2(\Omega))$, with $\gamma = \min\{s,\ 1-\delta\}$, for all $\delta > 0$ and space

$$H_0^\nu(0,T) := \{u \in H^\nu(0,T) \mid u(0) = u'(0) = 0\}.$$

Using condition (3.8), one can obtain the following:

$$\varrho(g^k) - V_k^\delta \to \varrho(g^\#) - V^\delta \quad \text{in}\ \ X^{\nu,s}(0,T;\ L^2(\Omega)) \quad \text{as}\ \ k \to \infty.$$

Consequently, we obtain the desired result

$$\|\varrho(g^\#) - V^\delta\|^2_{L^2(\Omega)} \le \liminf_{k\to+\infty} \left(\|\varrho(g^k) - V_k^\delta\|^2_{L^2(\Omega)}\right). \tag{3.11}$$

An application of Proposition 3.4 (see [13]) yields

$$Q(g^\#) = \left\|\varrho(g^\#) - V^\delta\right\|^2_{L^2(\Omega)} + \eta\|g^\#\|^2_{L^2(\Omega)} \le Q(g), \quad \forall g \in L^2(\Omega). \tag{3.12}$$

This result implies that g^* coincides with $g^\#$.

To prove the strong convergence of the sequence $\{g^k\}_{k\ge1}$ in $L^2(\Omega)$, we argue by contradiction. Suppose that the convergence is not strong. Then

$$\|g^k\|_{L^2(\Omega)} \not\longrightarrow \|g^*\|_{L^2(\Omega)} \quad \text{as}\ k \to \infty.$$

However, since $g^k \rightharpoonup g^*$ weakly in $L^2(\Omega)$ and the norm in $L^2(\Omega)$ is weakly lower semicontinuous, we have

$$\|g^*\|_{L^2(\Omega)} \le \liminf_{k\to\infty} \|g^k\|_{L^2(\Omega)} < \limsup_{k\to\infty} \|g^k\|_{L^2(\Omega)}, \tag{3.13}$$

which implies that the subsequence $\{g^k\}_{k\ge1}$ of $\{g^m\}_{m\ge1}$ satisfies

$$\limsup_{m\to\infty} \|g^m\|_{L^2(\Omega)} = \lim_{k\to\infty} \|g^k\|_{L^2(\Omega)}.$$

Using the characterization of the minimizing sequence $\{g^k\}_{k\ge1}$ and Eq (3.12), one may obtain

$$\begin{aligned}
\|\varrho(f^*) - V^\delta\|^2_{L^2(\Omega)} + \eta\|g^*\|^2_{L^2(\Omega)} &= \liminf_{k\to\infty} \left(\|\varrho(g^k) - V_k^\delta\|^2_{L^2(\Omega)} + \eta\|g^k\|^2_{L^2(\Omega)}\right) \\
&= \liminf_{k\to\infty} \left(\|\varrho(g^k) - V_k^\delta\|^2_{L^2(\Omega)} + \eta \limsup_{k\to\infty} \|g^k\|^2_{L^2(\Omega)}\right).
\end{aligned}$$

By inequality (3.13), one can deduce

$$\begin{aligned}
\|\varrho(g^*) - V^\delta\|^2_{L^2(\Omega)} &= \liminf_{k\to\infty} \|\varrho(g^k) - V_k^\delta\|^2_{L^2(\Omega)} + \eta \left((\limsup_{m\to\infty} \|f^m\|_{L^2(D)})^2 - \|f^*\|^2_{L^2(D)} \right) \\
&> \liminf_{k\to\infty} \|\varrho(g^k) - V_k^\delta\|^2_{L^2(\Omega)},
\end{aligned}$$

which leads to a contradiction with (3.11). □ □

This subsection is devoted to the sensitivity analysis of the cost functional Q with respect to the control variable g. Establishing the Fréchet differentiability of Q provides the theoretical foundation required for implementing gradient-based optimization techniques aimed at solving problem (3.4). In order to efficiently evaluate the gradient of Q, an adjoint formulation associated with (2.4) is introduced. The corresponding adjoint equation is expressed as a backward fractional parabolic problem, which significantly reduces the computational effort involved in the optimization process.

$$\begin{cases} {}^{RL}D_t^{\nu}P(x,t) = -(-\Delta)^s P(x,t), & (x,t) \in \Omega \times (0,T], \\ P = 0, & (x,t) \in \partial\Omega \times (0,T), \\ \lim\limits_{t\to T^-} \mathrm{I}_t^{2-\nu} P = 0, \quad \lim\limits_{t\to T^-} \dfrac{\partial}{\partial t}\mathrm{I}_t^{2-\nu} P = \left[\varrho(x,T) - V^{\delta}(x)\right], & (x,t) \in \Omega \times \{T\}. \end{cases} \tag{3.14}$$

In the following theorem, we prove that the functional Q is Fréchet differentiable and obtain a closed-form representation of its gradient.

Theorem 3.5. *The gradient of the function Q to be minimized is*

$$\nabla Q(g) = \left(\int_0^T h(t)P[g](x,t)\,dt + \eta g(x)\right). \tag{3.15}$$

The adjoint problem (3.14) *helps to deduce the value of* $P[g]$.

Proof. We consider $\delta g \in L^2(\Omega)$ as a small perturbation of g. Then, we have

$$\begin{aligned} Q(g+\delta g) - Q(g) &= \left\|\varrho[g+\delta g](.,T) - V^{\delta}(.)\right\|^2_{L^2(\Omega)} - \left\|\varrho[g](.,T) - V^{\delta}(.)\right\|^2_{L^2(\Omega)} \\ &\quad + \eta\,\|g+\delta g\|^2_{L^2(\Omega)} - \eta\,\|g\|^2_{L^2(\Omega)} + o\left(\|\delta g\|_{L^2(\Omega)}\right) \\ &= 2\int_{\Omega}\left(\varrho[g](.,T) - V^{\delta}(.)\right)\varrho[\delta g](.,T)\,dx \\ &\quad + 2\eta\int_{\Omega} g\delta g\,dx + o\left(\|\delta g\|_{L^2(\Omega)}\right). \end{aligned} \tag{3.16}$$

We have $\varrho[\delta g]$ as the solution to the problem

$$\begin{cases} {}^{C}D_t^{\nu}\varrho[\delta g] + (-\Delta)^s\varrho[\delta g] = \delta g(x)h(t) & \text{in } \Omega\times[0,T], \\ \varrho[\delta g] = 0 & \text{in } \partial\Omega\times[0,T], \\ \varrho[\delta g](x,0) = 0, \quad \dfrac{\partial\varrho[\delta g]}{\partial t}(x,0) = 0 & \text{in } \Omega. \end{cases} \tag{3.17}$$

Using (3.14) and (3.17), we have

$$\begin{aligned} \int_0^T\int_{\Omega} {}^{C}D_t^{\nu}\varrho[\delta g]\psi\,dx\,dt + \int_0^T B_s(\varrho[\delta g],\ \psi)\,dt = \int_0^T\int_{\Omega}\delta g(x)h(t)\psi(x,t)\,dx\,dt, \\ \forall\psi \in L^2\left((0,T);H_0^s(\Omega)\right). \end{aligned} \tag{3.18}$$

Similarly,

$$\int_0^T \int_\Omega {}^{RL}D_t^\gamma P[g]\psi \, dx\, dt + \int_0^T B_s(P[g],\ \psi)\, dt = \int_\Omega \Big(\varrho[g](.,T) - V^\delta(.)\Big)\varrho[\delta g](.,T)dx, \quad \forall \psi \in L^2\left((0,T); H_0^s(\Omega)\right). \tag{3.19}$$

Taking $\psi = P[g]$ in Eq (3.18) and using integration by parts, we have

$$\int_0^T \int_\Omega {}^{C}D_t^\gamma \varrho[\delta g] P[g]\, dx\, dt + \int_0^T B_s(\varrho[\delta g],\ P[g])\, dt = \int_0^T \int_\Omega \delta g(x) h(t) P[g](x,t)\, dx\, dt. \tag{3.20}$$

By replacing $\psi = \varrho[\delta g]$ with Eq (3.19), we deduce

$$\int_0^T \int_\Omega {}^{RL}D_t^\gamma P[g]\varrho[\delta g]\, dx\, dt + \int_0^T B_s(P[g],\ \varrho[\delta g])\, dt = \int_\Omega \Big(\varrho[g](.,T) - V^\delta(.)\Big)\varrho[\delta g](.,T)dx. \tag{3.21}$$

Hence,

$$\int_\Omega \Big(\varrho[g](.,T) - V^\delta(.)\Big)\varrho[\delta g](.,T)\, dx = \int_0^T \int_\Omega \delta g(x) h(t) P(x,t)\, dx\, dt. \tag{3.22}$$

Therefore,

$$\begin{aligned} Q(g+\delta g) - Q(g) &= \int_0^T \int_\Omega \delta g(x) h(t) P[g](x,t)\, dx\, dt + \int_\Omega g(x)\delta g(x)\, dx \\ &\quad + o\left(\|\delta g\|_{L^2(\Omega)}\right) \\ &= \int_0^T \int_\Omega h(t) P[g](x,t)\, dx\, dt + \eta \int_\Omega g(x)\delta g(x)\, dx + o\left(\|\delta g\|_{L^2(\Omega)}\right). \end{aligned} \tag{3.23}$$

Consequently, the gradient of Q is

$$\nabla Q(g) = \left(\int_0^T h(t) P[g](x,t)\, dt + \eta g(x)\right). \tag{3.24}$$

□

4. Numerical optimization using the conjugate gradient method

This section presents the computational strategy adopted to approximate the solution of the minimization problem. The methodology relies on the characterization of the solution through first-order optimality conditions and on their numerical resolution using a conjugate gradient based scheme. To compute the minimizer of the functional Q, we employ the CGM. Starting from an initial guess g^0, the iterative process generates $\{g^k\}$. If the approximation g^k is available at the k-th iteration, the update is performed according to the following iterative scheme.

$$g^{k+1} = g^k + \zeta_k d_k$$

with

$$d_k = \begin{cases} -\nabla Q(g^k) & \text{if } k = 0, \\ -\nabla Q(g^k) + \mu_k d_{k-1} & \text{if } k > 0, \end{cases}$$

and

$$\mu_k = \frac{\|\nabla Q(g^k)\|^2_{L^2(\Omega)}}{\|\nabla Q(g^{k-1})\|^2_{L^2(\Omega)}},$$

and

$$\zeta_k = \arg\min_{\zeta \geq 0} Q(g^k + \zeta d_k).$$

Then $Q(g^k + \zeta d_k)$ is expressed by

$$Q(g^k + \zeta d_k) = \left\|\Pi g^k + \zeta \Pi d_k - V^\delta\right\|^2_{L^2(\Omega)} + \eta \|g^k + \zeta d_k\|^2_{L^2(\Omega)}.$$

Differentiating $Q(g^k + \zeta d_k)$ with respect to ζ, we get

$$\frac{\partial Q(g^k + \zeta d_k)}{\partial \zeta} = \zeta \|\Pi d_k\|^2_{L^2(\Omega)} - \langle \Pi d_k,\ V^\delta \rangle_{L^2(\Omega)} + \langle \Pi d_k,\ \Pi g^k \rangle_{L^2(\Omega)} + \eta \zeta \|d_k\|^2_{L^2(\Omega)} + \eta \langle d_k,\ g^k \rangle_{L^2(\Omega)}.$$

The step size ζ_k is determined by

$$\frac{\partial Q(g^k + \zeta d_k)}{\partial \zeta} = 0,$$

which implies

$$\zeta_k = \frac{\langle \Pi d_k,\ V^\delta \rangle_{L^2(\Omega)} - \langle \Pi d_k,\ \Pi g^k \rangle_{L^2(\Omega)} - \eta \langle d_k,\ g^k \rangle_{L^2(\Omega)}}{\|\Pi d_k\|^2_{L^2(\Omega)} + \eta \|d_k\|^2_{L^2(\Omega)}}. \tag{4.1}$$

On the other hand, we have the following.

$$d_k = -\nabla Q(g^k) + \mu_k d_{k-1}, \quad q_k = -\nabla Q(g^k), \quad \text{and} \quad \langle q_k,\ d_{k-1} \rangle_{L^2(\Omega)} = 0.$$

Therefore,

$$\zeta_k = \frac{\|q_k\|^2_{L^2(\Omega)}}{\|\Pi d_k\|^2_{L^2(\Omega)} + \eta \|d_k\|^2_{L^2(\Omega)}}.$$

Furthermore, we consider the following CGM:

Algorithm 1 Conjugate Gradient Method

1: Set $k = 0$, initiate g^0.
2: Calculate $q_0 = \nabla Q(g^0)$ and set $d_0 = q_0$.
3: Evaluate

$$\zeta_0 = \frac{||q_0||^2_{L^2(\Omega)}}{||\Pi d_0||^2_{L^2(\Omega)} + \eta ||d_0||^2_{L^2(\Omega)}}.$$

4: Set $g^1 = g^0 + \zeta_0 d_0$.
5: **for** $k = 1, 2, \ldots$ **do**
6: Calculate

$$q_k = -\nabla Q(g^k), \quad d_k = q_k + \mu_k d_{k-1},$$

where

$$\mu_k = \frac{||q_k||^2_{L^2(\Omega)}}{||q_{k-1}||^2_{L^2(\Omega)}}.$$

7: Calculate

$$\zeta_k = \frac{||q_k||^2_{L^2(\Omega)}}{||\Pi d_k||^2_{L^2(\Omega)} + \eta ||d_k||^2_{L^2(\Omega)}}.$$

8: Update

$$g^{k+1} = g^k + \zeta_k d_k.$$

9: **end for**

5. Numerical approach using FEM

This section is concerned with the finite element approximation of the nonlinear optimization problem (3.4). A rigorous analysis of the convergence properties of the resulting numerical method is also provided. Assuming that Ω is a polyhedral domain, we triangulate Ω into a quasi-uniform mesh of regular shape $\mathcal{T}_\sigma$ with mesh size σ_x. In addition, we consider $W_\sigma \subset H_0^s(\Omega)$ to be the piecewise linear finite element space associated with $\mathcal{T}_\sigma$, namely,

$$W_\sigma := \{g_\sigma \in C(\overline{\Omega}) : g_\sigma|_K \in P_1(K), \quad \forall K \in \mathcal{T}_\sigma\}. \tag{5.1}$$

Here, $P_1(K)$ is the space of linear polynomials in the element K.

Let $g^\eta \in L^2(\Omega)$ be the unique solution of the optimization problem (3.4). Then g^η satisfies the equation:

$$\Pi^* \left(\Pi(g^\eta) - V\right) + \eta g^\eta = 0, \tag{5.2}$$

where $\Pi^* : L^2(\Omega) \to L^2(\Omega)$ is the adjoint operator of Π presented by

$$\Pi^* \vartheta = P,$$

where P is the solution of the adjoint problem (3.14).

For complete discretization, we introduce a uniform partition of the interval $[0, T]$: $0 = t_0 < t_1 < \cdots < t_N$, where $t_n = n\delta t$, $n = 0, 1, \cdots, N$ with the time step size $\delta t = T/N$.

Then, the fully discrete approximation for the fractional parabolic problem (3.4) by the backward Euler Galerkin method with initial datum $\varrho_\sigma^0[g] = 0$ is as follows: Find $\varrho_\sigma^n[g] \in W_\sigma$ for $n = 1, 2, \cdots, N$ such that

$$\langle\, {}^C D_t^\nu \varrho_\sigma^n[g],\ \Psi\rangle + B_s(\varrho_\sigma^n[g],\ \Psi) = \langle g h^n,\ \Psi\rangle \quad \forall \Psi \in W_\sigma, \tag{5.3}$$

where

$$\left[{}^C D_{a,x}^\nu \varrho\right]_{t=t_n} = \frac{1}{\Gamma(3-\nu)} \sum_{k=1}^{n-1} b_{n-k} \left[\varrho_\sigma^{k+1}[g] - 2\varrho_\sigma^k[g] + \varrho_\sigma^{k-1}[g]\right],\ n = 2, 3, \cdots, N,$$

with $b_{n-k} = \sigma^{-\nu} \cdot \dfrac{(n-k)^{2-\nu} - (n-k-1)^{2-\nu}}{2-\nu}$ and $h^n = h(t_n)$.

Problem (5.3) in its discrete variational form has a unique solution $\varrho_\sigma^n[g] \in W_\sigma$. Let $\varrho_\sigma[g](x,t)$ denote the piecewise linear interpolation in time of $\varrho_\sigma^n[g]$. Based on this approximation, we consider

$$\Pi_\sigma g := \varrho_\sigma[g](\cdot, T) \quad \text{in } \Omega.$$

Consequently, the approximation of (3.4) is ensured by

$$Q_\sigma(g) = \|\Pi_\sigma g - V\|_{L^2(\Omega)}^2 + \eta \|g\|_{L^2(\Omega)}^2 \ \longrightarrow\ \min. \tag{5.4}$$

The unique minimizer g_σ^η of this problem is defined by the following:

$$\Pi_\sigma^*(\Pi_\sigma g_\sigma^\eta - V) + \eta g_\sigma^\eta = 0, \tag{5.5}$$

where Π_σ^* denotes the adjoint operator of Π_σ.

To obtain a finite element approximation of (3.14), we introduce an approximate adjoint operator $\widehat{\Pi}_\sigma^*$ defined by

$$\widehat{\Pi}_\sigma^* \vartheta = P_\sigma, \qquad \vartheta \in L^2(\Omega). \tag{5.6}$$

Here, $P_\sigma \in W_\sigma$ stands for the discrete adjoint state uniquely determined by (3.14).

In practice, the exact final-time observation V is not available, and only noisy data V^δ are given. Replacing V with V^δ, we obtain the following discrete variational formulation:

$$\widehat{\Pi}_\sigma^* (\Pi_\sigma \widehat{g}_\sigma^\eta - V^\delta) + \eta \widehat{g}_\sigma^\eta = 0. \tag{5.7}$$

Finally, the influence of order s on the rate with respect to the spatial discretization parameter σ is investigated.

Lemma 5.1. *(See [22, Theorem 5.3]) Let $\varrho[g]$ and $\varrho_\sigma[g]$ be the solutions of problems* (3.1) *and* (5.3)*, respectively. Then there exists a constant $C > 0$, independent of the time and space discretization parameters, such that*

$$\|\varrho[g] - \varrho_\sigma[g]\|_{L^2(\Omega)} \le C\, M(t,\sigma)\, \|g\|_{L^2(\Omega)}, \tag{5.8}$$

where the function $M(t,\sigma)$ is defined as in [22, Theorem 5.3].

From Lemma 5.1, we deduce the following convergence results.

Theorem 5.1. *We have the following estimate.*

$$\|(\Pi_\sigma - \Pi)g\|_{L^2(\Omega)} = \mathcal{O}(M(t,\sigma)) \quad \textit{and} \quad \|(\widehat{\Pi}_\sigma^* - \Pi^*)g\|_{L^2(\Omega)} = \mathcal{O}(M(t,\sigma)).$$

Proof. Let $g \in L^2(\Omega)$ be arbitrary. By definition, the operator Π maps g to the solution $\varrho[g]$ of the continuous state problem (3.1), while Π_σ maps g to the fully discrete solution $\widehat{\varrho}_\sigma[g]$ of Eq (5.3). Therefore,

$$(\Pi_\sigma - \Pi)g = \widehat{\varrho}_\sigma[g] - \varrho[g].$$

Applying Lemma 5.1 directly to g, we obtain the estimate

$$\|\widehat{\varrho}_\sigma[g] - \varrho[g]\|_{L^2(\Omega)} \le C\, M(t,\sigma)\, \|g\|_{L^2(\Omega)}.$$

This immediately yields

$$\|(\Pi_\sigma - \Pi)g\|_{L^2(\Omega)} = \mathcal{O}(M(t,\sigma)).$$

To prove the second estimate, we use that Π^* and $\widehat{\Pi}_\sigma^*$ are adjoint operators of Π and Π_σ, respectively. For any $\vartheta \in L^2(\Omega)$, these adjoint operators are defined by

$$\langle \Pi g, \vartheta \rangle_{L^2(\Omega)} = \langle g, \Pi^* \vartheta \rangle_{L^2(\Omega)}, \qquad \langle \Pi_\sigma g, \vartheta \rangle_{L^2(\Omega)} = \langle g, \widehat{\Pi}_\sigma^* \vartheta \rangle_{L^2(\Omega)}.$$

Subtracting both identities gives

$$\langle (\Pi_\sigma - \Pi)g, \vartheta \rangle_{L^2(\Omega)} = \langle g, (\widehat{\Pi}_\sigma^* - \Pi^*)\vartheta \rangle_{L^2(\Omega)}.$$

Using the Cauchy-Schwarz inequality and the first part of the proof, we obtain

$$\left|\left\langle g, (\widehat{\Pi}^*_\sigma - \Pi^*)\vartheta\right\rangle\right| \le \|(\Pi_\sigma - \Pi)g\|_{L^2(\Omega)}\|\vartheta\|_{L^2(\Omega)} \le C\, M(t,\sigma)\, \|g\|_{L^2(\Omega)}\|\vartheta\|_{L^2(\Omega)}.$$

Since the above estimate holds for all $\vartheta \in L^2(\Omega)$, we conclude that

$$\|(\widehat{\Pi}^*_\sigma - \Pi^*)g\|_{L^2(\Omega)} = O(M(t,\sigma)).$$

□

Theorem 5.2. *Let $\eta > 0$. Then the following error estimate holds:*

$$\|g^\eta - \widehat{g}^\eta_\sigma\|_{L^2(\Omega)} \le C\, M(t,\sigma), \tag{5.9}$$

where g^η and $\widehat{g}^\eta_\sigma$ are the unique solutions of variational problems (5.2) *and* (5.7)*, respectively. The constant $C > 0$ can depend on g^η, V, and η but is independent of the discretization parameter σ.*

Proof. Taking into account the error $g^\eta - \widehat{g}^\eta_\sigma$, we arrive at the estimate (5.9). Equations (5.2) and (5.7) give us

$$\eta\,(g^\eta - \widehat{g}^\eta_\sigma) = \widehat{\Pi}^*_\sigma g^\eta_\sigma\,(\Pi_\sigma \widehat{g}^\eta_\sigma - V) - \Pi^*_\sigma g^\eta_\sigma \left(\Pi_\sigma g^\eta_\sigma - V^\delta\right). \tag{5.10}$$

Then,

$$\begin{aligned}
\eta^2 \left\|g^\eta - \widehat{g}^\eta_\sigma\right\|^2_{L^2(\Omega)} &= \left\langle \widehat{\Pi}^*_\sigma\,(\Pi_\sigma \widehat{g}^\eta_\sigma\ - V) - \Pi^*\left(\Pi_\sigma g^\eta - V^\delta\right) \widehat{g}^\eta_\sigma - g^\eta\right\rangle \\
&= \left\langle \widehat{\Pi}^*_\sigma \Pi_\sigma \widehat{g}^\eta_\sigma - \widehat{\Pi}^*_\sigma V - \Pi^*\Pi_\sigma g^\eta + \Pi^* V^\delta,\, \widehat{g}^\eta_\sigma - g^\eta\right\rangle \\
&= \left\langle \Pi^*\Pi_\sigma \widehat{g}^\eta_\sigma + (\widehat{\Pi}^*_\sigma - \Pi^*)\Pi_\sigma \widehat{g}^\eta_\sigma - \Pi^*\Pi_\sigma g^\eta + \Pi^* V^\delta - \widehat{\Pi}^*_\sigma V,\, \widehat{g}^\eta_\sigma - g^\eta\right\rangle \\
&= \langle \Pi^*\Pi_\sigma(\widehat{g}^\eta_\sigma - g^\eta),\, \widehat{g}^\eta_\sigma - g^\eta\rangle \\
&\quad + \left\langle (\widehat{\Pi}^*_\sigma - \Pi^*)\Pi_\sigma \widehat{g}^\eta_\sigma,\, \widehat{g}^\eta_\sigma - g^\eta\right\rangle \\
&\quad + \left\langle \Pi^*(V^\delta - V),\, \widehat{g}^\eta_\sigma - g^\eta\right\rangle \\
&\quad + \left\langle (\Pi^* - \widehat{\Pi}^*_\sigma)V,\, \widehat{g}^\eta_\sigma - g^\eta\right\rangle.
\end{aligned} \tag{5.11}$$

The first term on the right-hand side of the last identity can be estimated by combining (5.10) with Theorem 5.1, yielding

$$\begin{aligned}
\left\langle (\widehat{\Pi}^*_\sigma - \Pi^*)\Pi_\sigma \widehat{g}^\eta_\sigma,\ g^\eta_\sigma - \widehat{g}^\eta_\sigma\right\rangle &= \left\langle (\widehat{\Pi}^*_\sigma - \Pi^*)\Pi_\sigma(\widehat{g}^\eta_\sigma - g^\eta_\sigma),\ g^\eta_\sigma - \widehat{g}^\eta_\sigma\right\rangle \\
&\quad + \left\langle (\widehat{\Pi}^*_\sigma - \Pi^*)\Pi_\sigma g^\eta_\sigma,\ g^\eta_\sigma - \widehat{g}^\eta_\sigma\right\rangle \\
&\le \left\|(\widehat{\Pi}^*_\sigma - \Pi^*)\Pi_\sigma(\widehat{g}^\eta_\sigma - g^\eta_\sigma)\right\|_{L^2(\Omega)} \left\|g^\eta_\sigma - \widehat{g}^\eta_\sigma\right\|_{L^2(\Omega)} \\
&\quad + \left\|(\widehat{\Pi}^*_\sigma - \Pi^*)\Pi_\sigma g^\eta_\sigma\right\|_{L^2(\Omega)} \left\|g^\eta_\sigma - \widehat{g}^\eta_\sigma\right\|_{L^2(\Omega)} \\
&\le C_2 M(t,\sigma) \left\|g^\eta_\sigma - \widehat{g}^\eta_\sigma\right\|^2_{L^2(\Omega)} \\
&\quad + C_3 M(t,\sigma) \left\|V^\delta\right\|_{L^2(\Omega)} \left\|g^\eta_\sigma - \widehat{g}^\eta_\sigma\right\|_{L^2(\Omega)}.
\end{aligned}$$

Similarly, the second term can be estimated by applying inequality (5.10) together with Theorem 5.1.

$$\begin{aligned}\langle \Pi^*\Pi_\sigma\widehat{g}_\sigma^\eta - \Pi_\sigma^*\Pi_\sigma g_\sigma^\eta,\ g_\sigma^\eta - \widehat{g}_\sigma^\eta\rangle &= \langle \Pi_\sigma\widehat{g}_\sigma^\eta,\ \Pi(g_\sigma^\eta - \widehat{g}_\sigma^\eta)\rangle - \langle \Pi_\sigma g_\sigma^\eta,\ \Pi_\sigma(g_\sigma^\eta - \widehat{g}_\sigma^\eta)\rangle \\ &= \langle \Pi_\sigma(\widehat{g}_\sigma^\eta - g_\sigma^\eta),\ \Pi_\sigma(\widehat{g}_\sigma^\eta - g_\sigma^\eta)\rangle + \langle \Pi_\sigma g_\sigma^\eta,\ (\Pi - \Pi_\sigma)(g_\sigma^\eta - \widehat{g}_\sigma^\eta)\rangle \\ &= \langle (\Pi_\sigma - \Pi)(\widehat{g}_\sigma^\eta - g_\sigma^\eta),\ \Pi(g_\sigma^\eta - \widehat{g}_\sigma^\eta)\rangle - \left\|\Pi(g_\sigma^\eta - \widehat{g}_\sigma^\eta)\right\|_{L^2(\Omega)}^2 \\ &\quad + \langle \Pi_\sigma g_\sigma^\eta, (\Pi - \Pi_\sigma)(g_\sigma^\eta - \widehat{g}_\sigma^\eta)\rangle \\ &\le C_3 M(t,\sigma)\left\|g_\sigma^\eta - \widehat{g}_\sigma^\eta\right\|_{L^2(\Omega)}^2 \\ &\quad + C_4 M(t,\sigma)\left\|V\right\|_{L^2(\Omega)}\left\|g_\sigma^\eta - \widehat{g}_\sigma^\eta\right\|_{L^2(\Omega)}.\end{aligned}$$

Finally, applying inequality (3.4) together with Theorem 5.1, we obtain the following.

$$\begin{aligned}\langle \Pi_\sigma^* V^\delta - \widehat{\Pi}_\sigma^*,\ g_\sigma^\eta - \widehat{g}_\sigma^\eta\rangle &= \langle (\Pi - \Pi_\sigma^*)V,\ g_\sigma^\eta - \widehat{g}_\sigma^\eta\rangle + \langle V^\delta - V,\ \Pi(g_\sigma^\eta - \widehat{g}_\sigma^\eta)\rangle \\ &\quad + \langle V^\delta,\ (\Pi_\sigma - \Pi) - (g_\sigma^\eta - \widehat{g}_\sigma^\eta)\rangle \\ &\le C_6 M(t,\sigma)\|g_\sigma^\eta - \widehat{g}_\sigma^\eta\|_{L^2(\Omega)}.\end{aligned}$$

Hence,

$$\|g_\sigma^\eta - \widehat{g}_\sigma^\eta\|_{L^2(\Omega)} \le C_7(M(t,\sigma) + \delta). \tag{5.12}$$

Using the same arguments as in (5.11), we obtain

$$\eta^2 \left\|g^\eta - \hat{g}_\sigma^\eta\right\|_{L^2(\Omega)}^2 \le C_8 M(t,\sigma) \left\|g^\eta - \hat{g}_\sigma^\eta\right\|_{L^2(\Omega)}.$$

This completes the proof of the theorem. □

6. Numerical experiments and results

Convergence study of the FEM projection. In this experiment, we investigate the spatial convergence behavior of the finite element approximation obtained by the P_1 finite element method. More precisely, we consider the L^2-projection of the exact solution to (2.4),

$$\varrho_{\mathrm{ex}}(x,t) = (1 + t^\nu)\, C_s\, (1 - x^2)^s\, \chi_{(-1,1)}(x), \quad C_s = \frac{\sqrt{\pi}\, 2^{-2s}}{\Gamma\left(s + \frac{1}{2}\right)\Gamma(s+1)},$$

onto the finite element space defined on a uniform partition of the interval $(-1, 1)$. The error is evaluated at the fixed time $t = 0.5$ for $\nu = 1.6$ and $s = 0.3$.

Table 1 reports the L^2-errors between the exact solution and its finite element approximation for several mesh sizes h. The corresponding convergence rates are computed using successive mesh refinements. As observed from the table, the L^2-error decreases monotonically as the mesh is refined.

Table 1. Evolution of the L^2-error for the FEM P_1 projection at $t = 0.5$ with $\nu = 1.6$ and $s = 0.3$.

h	L^2-error	Relative L^2-error
8.0000×10^{-2}	9.205217×10^{-2}	5.027488×10^{-2}
4.0000×10^{-2}	5.280715×10^{-2}	2.884104×10^{-2}
2.0000×10^{-2}	3.031206×10^{-2}	1.655518×10^{-2}
1.0000×10^{-2}	1.740468×10^{-2}	9.505716×10^{-3}
6.6667×10^{-3}	1.258205×10^{-2}	6.871797×10^{-3}
5.0000×10^{-3}	9.994932×10^{-3}	5.458817×10^{-3}

Furthermore, Figure 1 illustrates the evolution of the L^2-error as a function of the mesh size h on a logarithmic scale. The numerical results exhibit an experimental convergence rate close to $O(h^{0.8})$, which is consistent with the reduced regularity of the exact solution near the boundary due to the fractional power $(1 - x^2)^s$. This confirms the theoretical expectation that the convergence order of the P_1 finite element approximation depends on the fractional exponent s.

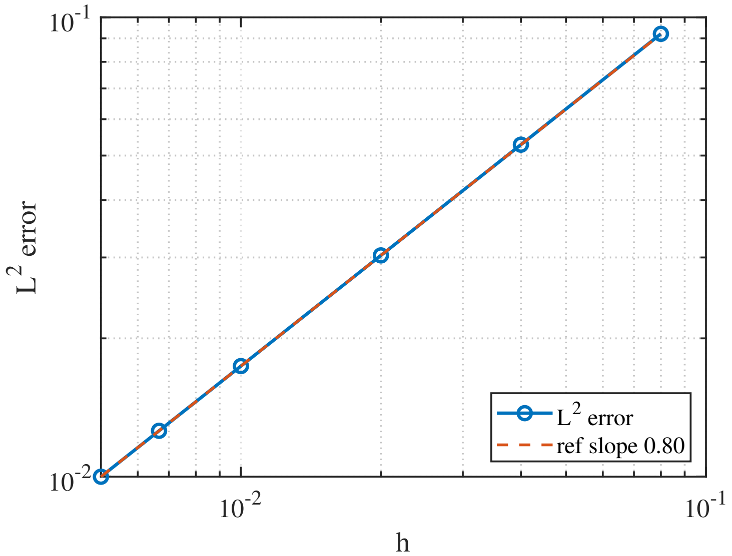

Figure 1. Evolution of the L^2-error with respect to the mesh size h.

Overall, these results demonstrate the reliability and accuracy of the proposed finite element projection scheme for approximating fractional-type solutions in the L^2 sense.

Comparison between exact and approximate solutions. To further illustrate the accuracy of the proposed Nyström-based discretization, we plot in Figure 2 the exact solution $\varrho_{\text{exact}}(x, t)$ and its numerical approximation $\varrho_{\text{num}}(x, t)$ at a fixed time $t = 0.5$. An excellent agreement between the numerical and exact solutions is observed over the entire domain, confirming the robustness and accuracy of the forward solver.

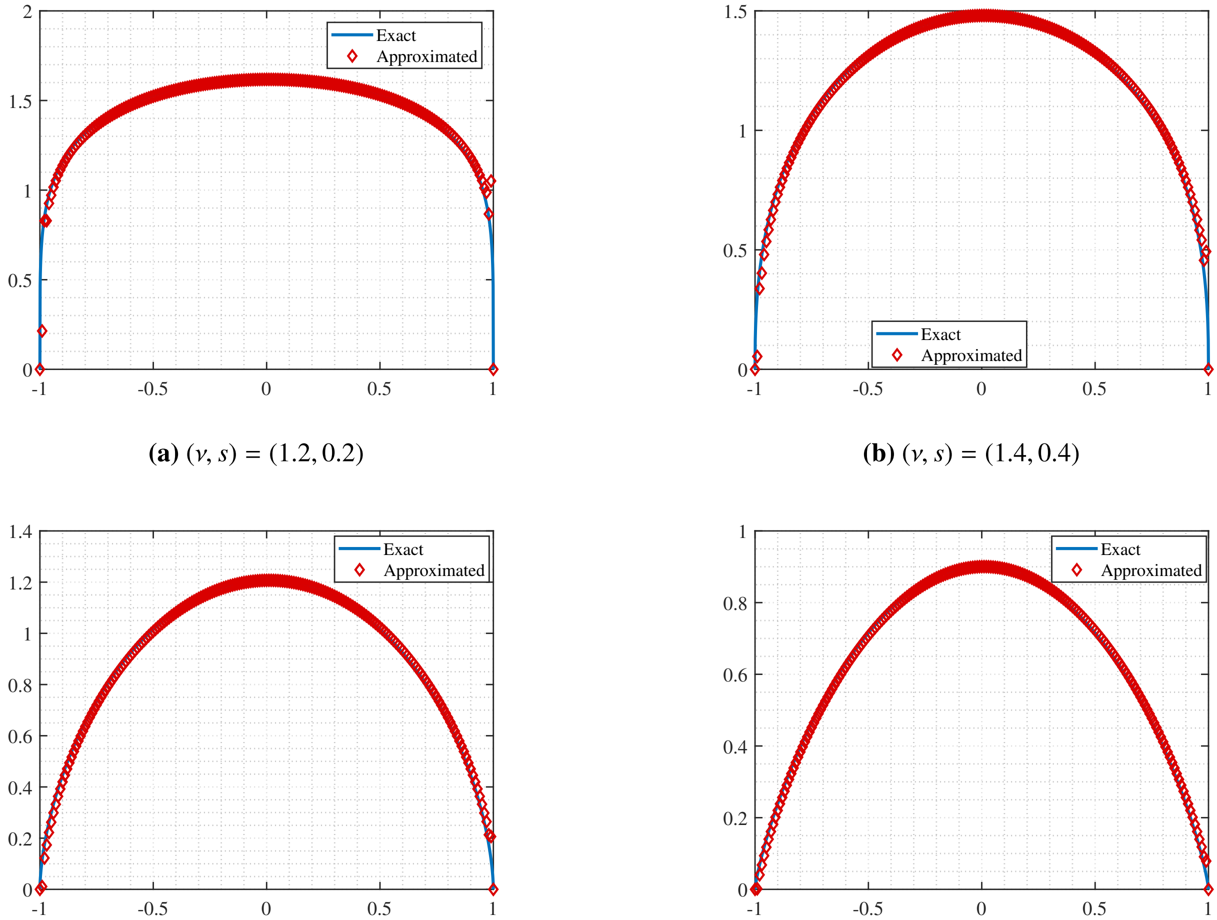

(a) $(\nu, s) = (1.2, 0.2)$

(b) $(\nu, s) = (1.4, 0.4)$

(c) $(\nu, s) = (1.6, 0.8)$

(d) $(\nu, s) = (1.8, 0.8)$

Figure 2. Exact and approximate solutions at time $t = 0.5$ for different values of the fractional orders.

6.1. Numerical experiments and implementation details for the inverse problem

This section explores the numerical validation of the CGM developed in the previous sections. A series of numerical experiments is carried out to assess the accuracy, stability, and efficiency of the proposed reconstruction algorithm. Throughout the experiments, the spatial domain is chosen as $\Omega = (-1, 1)$, and the final time $T > 0$ is fixed. Additional input functions and parameters are specified individually for each test case.

At every iteration of the inverse algorithm, the forward problem (3.1) together with its corresponding adjoint problem (3.14) must be computed numerically. For this purpose, a fully discrete formulation is adopted, in which the time variable is approximated using a finite difference scheme, while the spatial discretization of the fractional Laplacian is performed using the finite element method, following the approach in [23]. The domain Ω is uniformly divided into $N = 50$ subintervals with mesh size $h = 1/N$. The time interval $(0, T)$ is discretized using a uniform time step $\zeta = 1/M$, where $M = 1000$.

A primary goal of these experiments is to show the capability of the established algorithm to accurately reconstruct the unknown $g(x)$ in problem (3.1) from final-time observation data $\varrho(\cdot, T) = V$. To quantify the reconstruction quality, we compute the $L^2(\Omega)$-error using the source g_{exact} and its numerical approximation g_k obtained after k iterations, defined by

$$E_k = \|g_{\text{exact}} - g_k\|_{L^2(\Omega)}.$$

In practical applications, measurement data are inevitably affected by noise. To simulate this situation, noisy observations are generated by adding

$$V^\delta = V + \epsilon V(2\,\text{rand}(\text{size}(V)) - 1), \quad x \in \Omega, \tag{6.1}$$

where $\epsilon > 0$ controls the noise amplitude. The corresponding noise level is measured by

$$\delta = \|V^\delta - V\|_{L^2(\Omega)}.$$

We define the residual at the k-th iteration by

$$R_k = \left\|\varrho(g^k) - V^\delta\right\|_{L^2(\Omega)}.$$

Example 6.1. In the first numerical test, the exact source is assumed to be smooth and is defined by

$$g_{\text{exact}}(x) = \sin(\pi x),$$

together with the time-dependent function

$$h(t) = 10(t^2 + 1)\cos(\pi t)$$

and the initial condition

$$\varrho_0(x) = \cos(2\pi x)(x^2 - 1).$$

The final observation data $V(x) = \varrho(x, T)$ are generated by solving the forward problem (3.1). CGM is then applied to reconstruct the unknown source term from noisy final-time measurements. Numerical reconstructions are carried out for different noise levels δ, considering the fractional parameters $\nu = 1.6$ and $s = 0.8$. The corresponding reconstruction results and convergence behavior are illustrated in Figures 3 and 4.

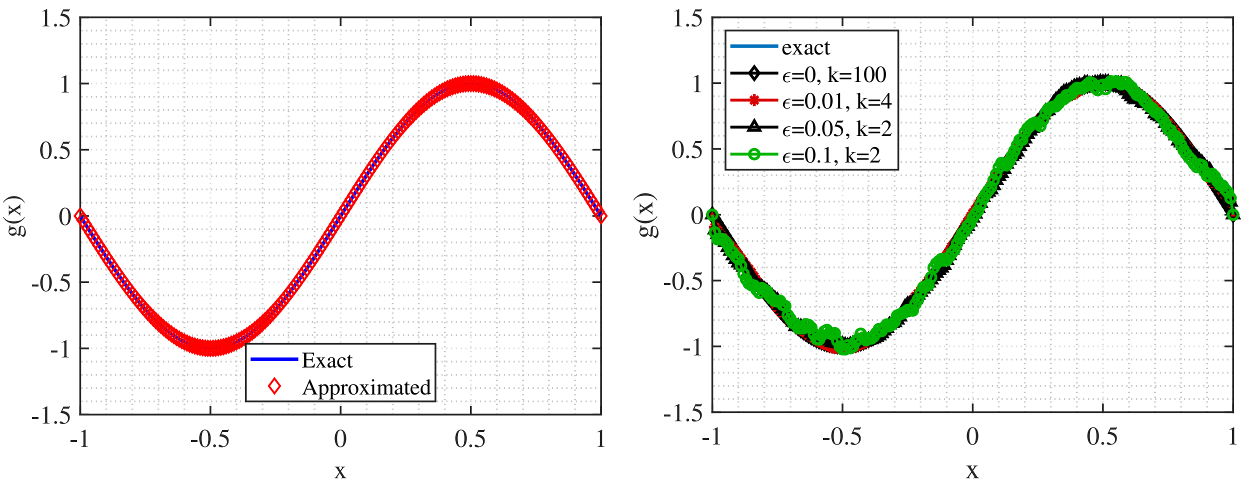

(a) Exact and reconstructed solution

(b) Numerical results at different noise levels

Figure 3. Numerical results with $k = 80$ and $\eta = 10^{-3}$.

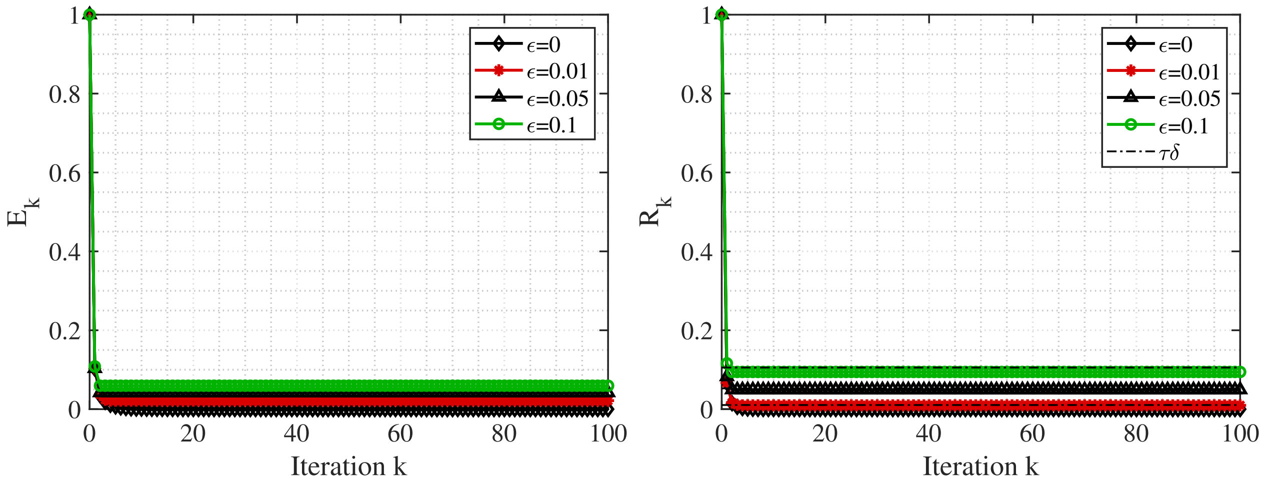

(a) Error E_k^2 **(b)** Residual $\mathcal{R}_k$

Figure 4. Numerical results with $k = 100$ and $\eta = 10^{-3}$.

Example 6.2. In this example, we investigate the performance of the proposed method for a non smooth source function. The exact source term is chosen as

$$g_{\text{exact}}(x) = 1 - |x|,$$

while the time-dependent function is given by

$$h(t) = e^{-t},$$

and the initial condition is

$$\varrho_0(x) = x^2 - 1.$$

The final observation data $V(x) = \varrho(x, T)$ are generated by numerically solving the forward problem (3.1). The reconstruction results obtained for different noise levels are displayed in Figures 5 and 6.

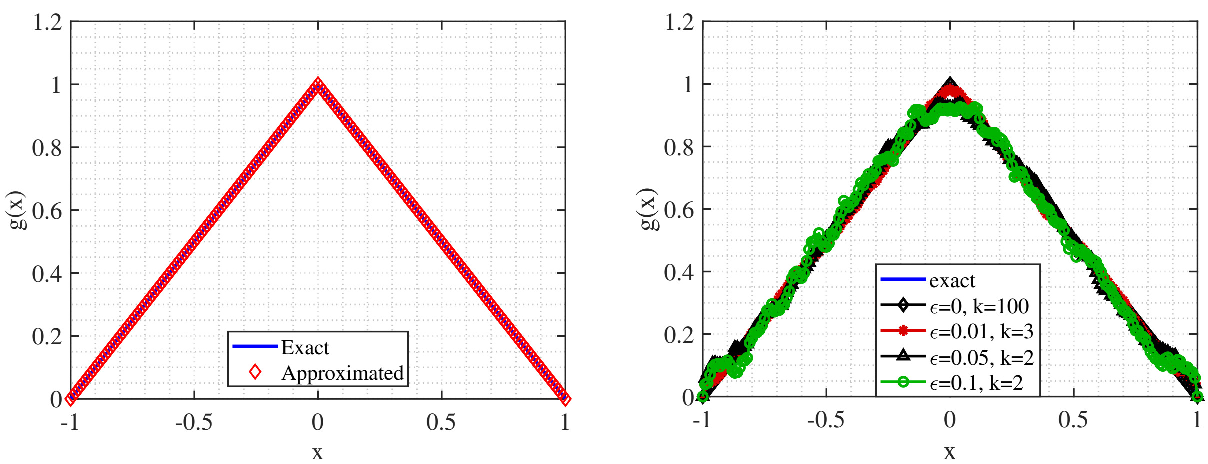

(a) Exact and reconstructed solution **(b)** Numerical results at different noise levels

Figure 5. Numerical results with $k = 100$ and $\eta = 10^{-3}$.

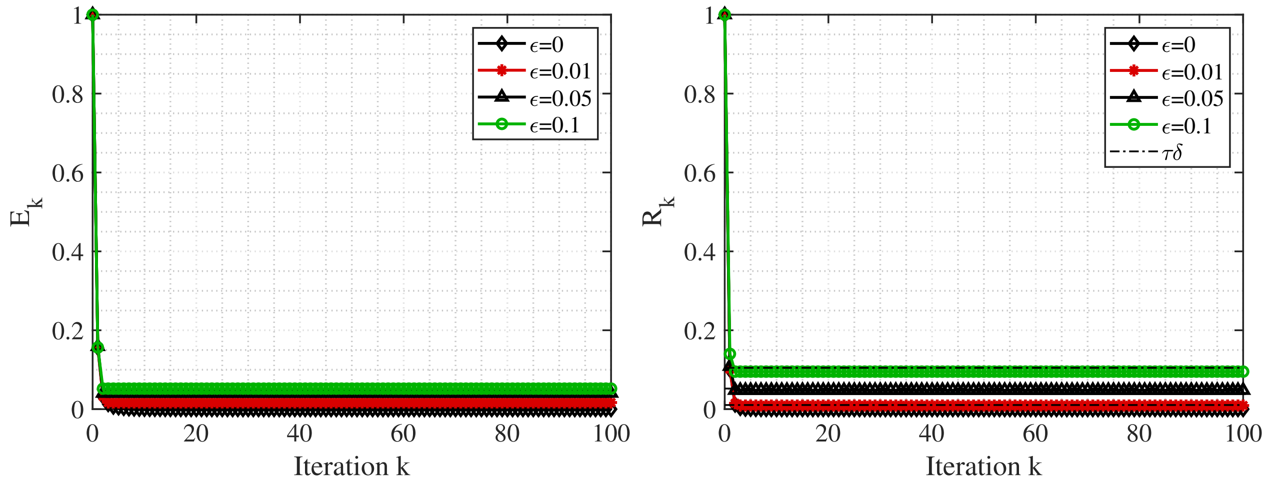

(a) Error E_k^2 **(b)** Residual $\mathcal{R}_k$

Figure 6. Numerical results with $k = 100$ and $\eta = 10^{-3}$.

Example 6.3. In this last example, we seek to identify the non smooth source term given by

$$g_{exact}(x) = \begin{cases} 0, & x \in [-1, -0.75) \cup (0.75, 1], \\ 1, & x \in [-0.75, -0.25) \cup (0.25, 0.75], \\ 2, & x \in [-0.25, 0.25], \end{cases}$$

and the rest of the definite input functions are the same as in the previous example. The final data $V(x) = \varrho(x, T)$ are obtained by solving the forward problem (3.1). The numerical results for this example are illustrated for various noise levels in Figures 7 and 8.

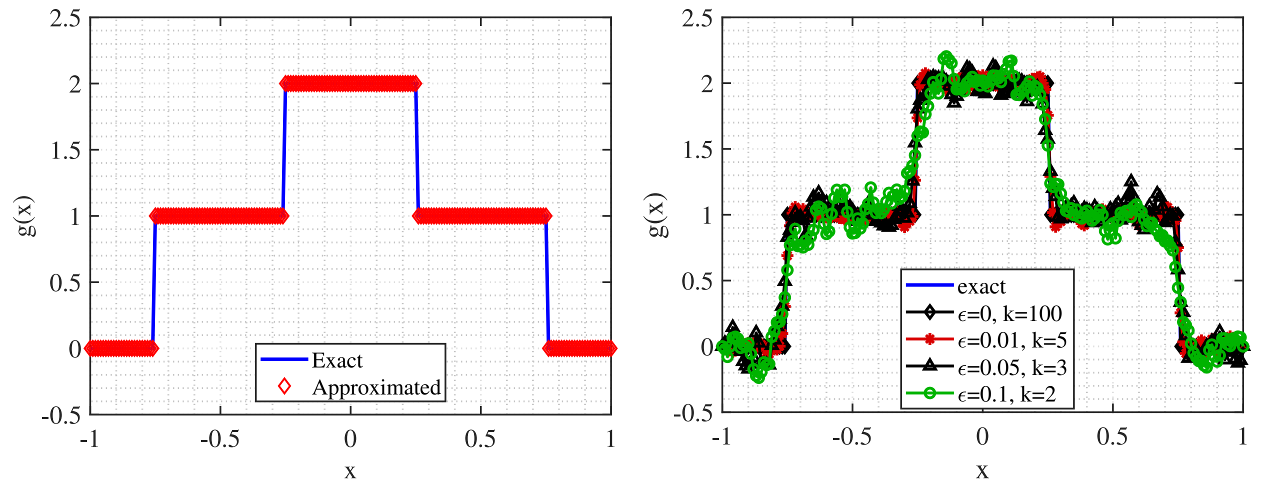

(a) Exact and reconstructed solution **(b)** Numerical results at different noise levels

Figure 7. Numerical results with $k = 100$ and $\eta = 10^{-3}$.

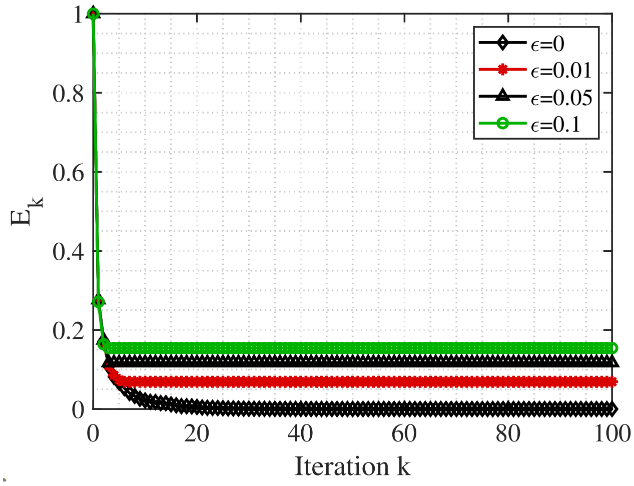

(a) Exact and reconstructed solution

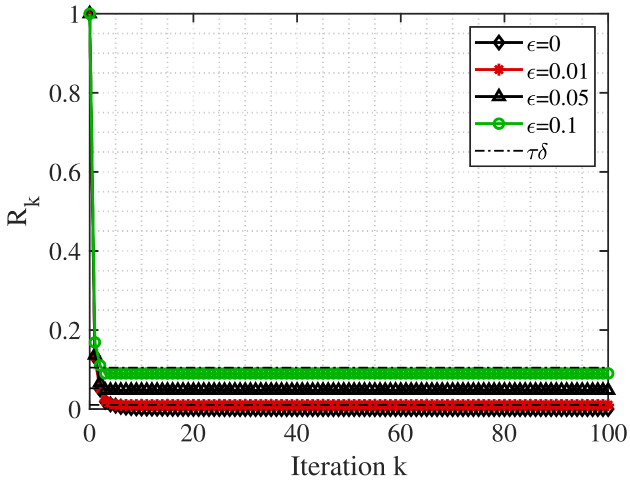

(b) Numerical results at different noise levels

Figure 8. Numerical results with $k = 100$ and $\eta = 10^{-3}$.

A.1. Dependence of the reconstruction accuracy on the fractional orders

To quantify the influence of the fractional parameters on the reconstruction, we identify the source $g_{\text{exact}} = 1-|x|$ a nonsmooth, piecewise-linear source chosen to probe the sensitivity of the reconstruction from its final-time data while varying the temporal order $\nu \in (1, 2)$ and the spatial order $s \in (0, 1)$ independently. All remaining data are fixed: $h(t) = e^{-t}$, $T = 1$, the mesh size ($N = 160$), the time step, the regularization parameter $\eta = 10^{-3}$, and the stopping rule. The reconstruction error is $E = \|g_{ex} - g_k\|_{L^2(\Omega)}$.

As seen in Table A.1 and Figure A.1, the error grows substantially with the spatial order s by roughly an order of magnitude from $s = 0.2$ to $s = 0.8$ whereas it varies only mildly, and decreases slightly, as ν approaches the wave regime. This reflects the fact that the smoothing strength of the forward operator, and hence the degree of ill-posedness of the inverse problem, is governed primarily by s.

Table A.1. Reconstruction error E as a function of the fractional orders.

(a) fixed $s = 0.5$, varying ν		
ν	$E = \|g_{\text{exact}} - g_k\|_{L^2(\Omega)}$	Relative L^2-error
1.2	2.097263×10^{-2}	2.568612×10^{-2}
1.4	1.947841×10^{-2}	2.385609×10^{-2}
1.6	1.844295×10^{-2}	2.258791×10^{-2}
1.8	1.674696×10^{-2}	2.051076×10^{-2}

(b) fixed $\nu = 1.6$, varying s		
s	$E = \|g_{\text{exact}} - g_k\|_{L^2(\Omega)}$	Relative L^2-error
0.2	5.281407×10^{-3}	6.468377×10^{-3}
0.4	1.044055×10^{-2}	1.278701×10^{-2}
0.6	2.882589×10^{-2}	3.530436×10^{-2}
0.8	5.863309×10^{-2}	7.181057×10^{-2}

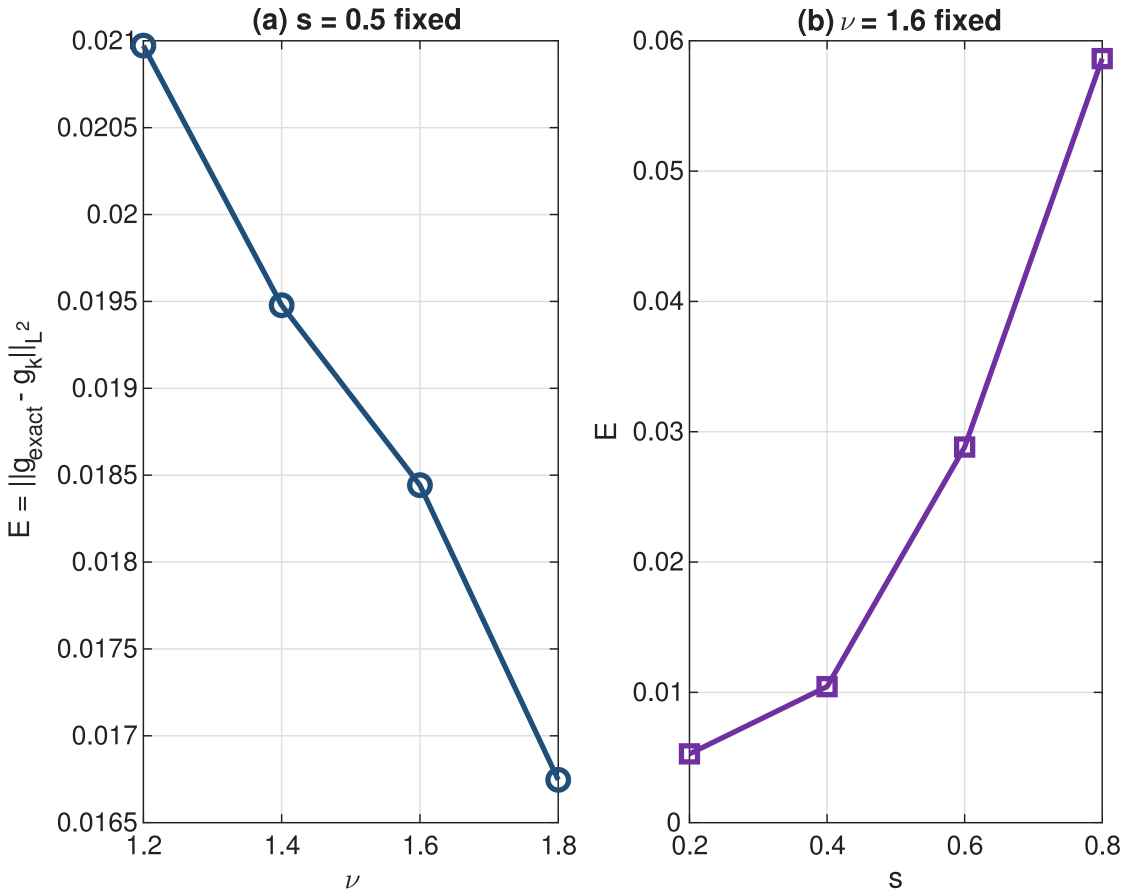

Figure A.1. Reconstruction error E versus the temporal order ν (left, $s = 0.5$ fixed) and versus the spatial order s (right, $\nu = 1.6$ fixed).

A.2. Convergence order of the inverse solver for noise-free data

In Table A.2, we study the convergence of the reconstruction with respect to the mesh size h in the noise-free regime $\delta = 0$. The source is taken smooth, $g_{\text{exact}} = \sin(\pi x)$, with the orders $\nu = 1.6$, $s = 0.3$ of Table 1, so that the observed rate reflects the discretization of the operator rather than the limited regularity of the source (in contrast with the nonsmooth source used in Appendix A.1 to probe sensitivity). As noted above, for a fixed regularization parameter, the meaningful discretization quantity is $E = \|g^\eta - \widehat{g}^\eta_\sigma\|_{L^2(\Omega)}$, the error between the discrete reconstruction $\widehat{g}^\eta_\sigma$, and the continuous regularized solution g^η. Since g^η has no closed form, it is approximated on a fine reference mesh ($N = 1280$): The noise-free data are computed on this fine mesh and sampled on each coarse mesh so that data generation and inversion use *different* meshes, which rules out an inverse crime and the coarse reconstruction is then compared with the fine-mesh regularized solution. The experimental order of convergence is $p_i = \ln(E_i/E_{i+1})/\ln(h_i/h_{i+1})$.

Figure A.2 show that the error decreases monotonically, and the experimental order approaches $O(h)$, in agreement with the estimate of Theorem 5.2. This confirms that the discrete reconstruction inherits the convergence predicted by the analysis of Section 5.

Table A.2. Evolution of the L^2-error of the reconstruction under mesh refinement (noise-free data, $\nu = 1.6$, $s = 0.3$).

h	L^2-error	Relative L^2-error	EOC
8.0000×10^{-2}	1.680653×10^{-2}	1.7052×10^{-2}	—
4.0000×10^{-2}	1.506142×10^{-2}	1.5221×10^{-2}	0.158
2.0000×10^{-2}	9.120209×10^{-3}	9.2072×10^{-3}	0.724
1.0000×10^{-2}	4.449848×10^{-3}	4.4911×10^{-3}	1.035
6.6667×10^{-3}	3.056955×10^{-3}	3.0852×10^{-3}	0.926
5.0000×10^{-3}	2.265976×10^{-3}	2.2868×10^{-3}	1.041

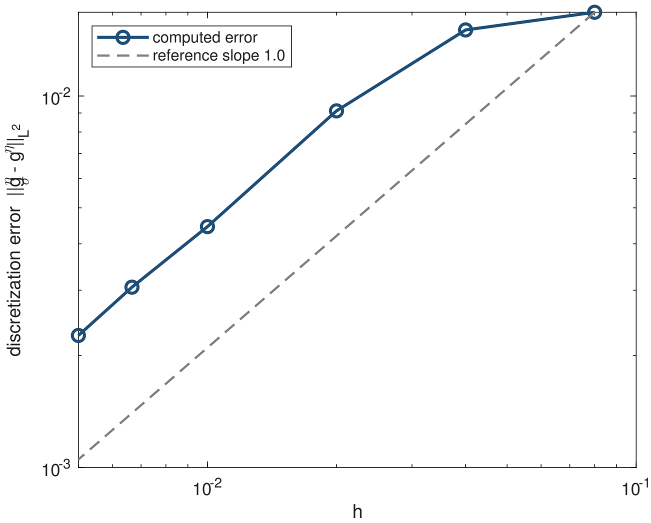

Figure A.2. Convergence of the discretization error of the reconstruction with respect to the mesh size h (noise-free data), on a logarithmic scale.

6.2. *Reconstruction without noise*

The results of the reconstruction procedure for the previous three examples without noise are illustrated in Figures 3(a), 4(a) and 5(a), in which we plot the exact and reconstructed solution for comparison. As can be seen from these figures, the design provides very close and accurate solutions without noise, i.e., $\delta = 0$ for both cases: A regular and non smooth function.

6.3. *Reconstruction with noise*

Now, we examine the effect of the noise level on the precision of the reconstruction algorithm, which can be done by considering the exact final measurement and adding some noise level given by formula (6.1). In Figures 4, 6 and 8, we present the results obtained with different noise levels for Examples (6.1), (6.2) and (6.3), respectively. The obtained results, for both cases of smooth and non-smooth solutions, make clear that the CGM is suitable for such kinds of issues, which provides stable and accurate numerical results in the presence of noise in measurement data. However, it should be noted that for a high noise level (more than 5%), the accuracy of the solutions can definitely be lost.

7. Conclusions

In this study, we focused on the optimal recovery of spatial sources for a dynamical problem characterized by a space–time fractional diffusion–wave model. We addressed the inverse problem of identifying a space-dependent source term based on noisy final-time observations. Our contributions included both theoretical insights and numerical solutions. We proved the existence and uniqueness of solutions to the direct and inverse problems and tackled the ill-posedness of the inverse formulation by reformulating it as an optimization problem within the Tikhonov regularization framework. We provided a comprehensive analysis of the well-posedness of the regularized problem, including stability and uniqueness results. To efficiently compute approximate solutions, we developed a conjugate gradient algorithm based on the corresponding adjoint problem. The effectiveness and accuracy of the proposed approach were validated through several one-dimensional numerical experiments, confirming its robustness and practical applicability to solving inverse source problems within fractional-order dynamical systems.

Author contributions

All authors contributed equally to this work. All authors have read and approved the final version of the manuscript for publication.

Use of Generative-AI tools declaration

The authors declare they have not used Artificial Intelligence (AI) tools in the creation of this article.

Data availability

The simulated data used in the article are available from the corresponding author.

Acknowledgments

This work was funded by the Deanship of Graduate Studies and Scientific Research at Jouf University under Grant No. (DGSSR-2024-02-02056).

Conflicts of interest

The authors declare that they have no conflict of interest.

References

1. E. Valdinoci, From the long jump random walk to the fractional Laplacian, *arXiv preprint*, 2009, arXiv:0901.3261.
2. M. M. Meerschaert, D. A. Benson, H. P. Scheffler, B. Baeumer, Stochastic solution of space-time fractional diffusion equations, *Phys. Rev. E*, **65** (2002), 041103.

3. C. J. Weiss, B. G. van Bloemen-Waanders, H. Antil, Fractional operators applied to geophysical electromagnetics, *Geophys. J. Int.*, **220** (2020), 1242–1259.

4. H. Antil, C. N. Rautenberg, Sobolev spaces with non-muckenhoupt weights, fractional elliptic operators, and applications, *SIAM J. Math. Anal.*, **51**, (2019), 2479–2503. https://doi.org/10.1137/18M1224970

5. J. L. Vázquez, *Nonlinear diffusion with fractional laplacian operators*, in: Nonlinear partial differential equations: The Abel Symposium 2010, Springer, 2012, 271–298.

6. H. Antil, T. Berry, J. Harlim, Fractional diffusion maps, *Appl. Comput. Harmon. A.*, **54** (2021), 145–175.

7. S. Dipierro, G. Palatucci, E. Valdinoci, Dislocation dynamics in crystals: A macroscopic theory in a fractional laplace setting, *Commun. Math. Phys.*, **333** (2015), 1061–1105. https://doi.org/10.1007/s00220-014-2118-6

8. G. M. Viswanathan, V. Afanasyev, S. V. Buldyrev, E. J. Murphy, P. A. Prince, H. E. Stanley, Lévy flight search patterns of wandering albatrosses, *Nature*, **381** (1996), 413–415. https://doi.org/10.1038/381413a0

9. D. A. Murio, Implicit finite difference approximation for time fractional diffusion equations, *Comput. Math. Appl.*, **56** (2008), 1138–1145.

10. J. Nakagawa, K. Sakamoto, M. Yamamoto, Overview to mathematical analysis for fractional diffusion equations: New mathematical aspects motivated by industrial collaboration, 2010.

11. M. Andrle, A. El Badia, On an inverse source problem for the heat equation. Application to a pollution detection problem, II, *Inverse Probl. Sci. En.*, **23** (2015), 389–412. https://doi.org/10.1080/17415977.2014.906415

12. A. El Badia, T. Ha-Duong, An inverse source problem in potential analysis, *Inverse Probl.*, **16** (2000), 651. https://doi.org/10.1088/0266-5611/16/3/308

13. M. BenSaleh, H. Maatoug, Inverse source problem for a space-time fractional diffusion equation, *Ric. Mat.*, **73** (2024), 681–713. https://doi.org/10.1007/s11587-021-00632-x

14. H. O. Sidi, M. Zaky, K. Waled, A. Akgül, A. Hendy, Numerical reconstruction of a space-dependent source term for multidimensional space-time fractional diffusion equations, *Rom. Rep. Phys.*, **75** (2023), 120. https://doi.org/10.59277/RomRepPhys.2023.75.120

15. M. Ali, S. Aziz, S. A. Malik, Inverse source problems for a space–time fractional differential equation, *Inverse Probl. Sci. En.*, **28** (2020), 47–68. https://doi.org/10.1016/S0150-9861(20)30092-4

16. K. S. Miller, B. Ross, *An introduction to the fractional calculus and fractional differential equations*, Wiley, 1993.

17. K. Oldham, J. Spanier, *The fractional calculus theory and applications of differentiation and integration to arbitrary order*, Elsevier, 1974.

18. R. A. Adams, *Sobolev spaces*, New York, San Francisco. Lodon: Academic Press, **1** (1975), 975.

19. M. BenSalah, S. Tatar, Identification of the initial value for a space-time fractional diffusion equation, *arXiv preprint*, 2024, arXiv:2412.05387. https://doi.org/10.21203/rs.3.rs-4541317/v1

20. J. W. He, Y. Liang, B. Ahmad, Y. Zhou, Nonlocal fractional evolution inclusions of order $\alpha \in (1, 2)$, *Mathematics*, **7** (2019), 209. https://doi.org/10.3390/math7020209

21. M. Hrizi, M. BenSalah, M. Hassine, Determination of the initial density in nonlocal diffusion from final time measurements, *Discrete Cont. Dyn.-S*, **15** (2022), 1469. https://doi.org/10.3934/dcdss.2022029

22. G. Acosta, F. M. Bersetche, J. P. Borthagaray, Finite element approximations for fractional evolution problems, *Fract. Calc. Appl. Anal.*, **22** (2019), 767–794. https://doi.org/10.1515/fca-2019-0042

23. U. Biccari, V. Hernández-Santamaría, A finite element approximation of the one-dimensional fractional poisson equation with applications to numerical control, *arXiv preprint*, 2017, arXiv:1707.06769.

AIMS Press